

Novel calcium-regulating mechanism of barium-doped material for the treatment of neuropathic pain



Thesis submitted in partial fulfilment for the
Award of Degree

Doctor of Philosophy

By

Shreyasi Majumdar

DEPARTMENT OF PHARMACEUTICAL ENGINEERING & TECHNOLOGY
INDIAN INSTITUTE OF TECHNOLOGY
(BANARAS HINDU UNIVERSITY) VARANASI-
221005
INDIA

Roll No.18161005

2024

CERTIFICATE

It is certified that the work contained in the thesis titled “**Novel calcium-regulating mechanism of barium-doped material for the treatment of neuropathic pain**” by Ms. **Shreyasi Majumdar** has been carried out under my supervision and that this work has not been submitted elsewhere for a degree.

It is further certified that the student has fulfilled all the requirements of Comprehensive Examination, Candidacy, and SOTA for the award of Ph.D. Degree.

Date:

Place: IIT (BHU), Varanasi

SK
17/3/24

Prof. Sairam Krishnamurthy

(Supervisor)

Prof. SAIRAM KRISHNAMURTHY
Dept. of Pharm. Engg. & Tech.
Indian Institute of Technology
(Banaras Hindu University)
Varanasi-221005 (U.P.)

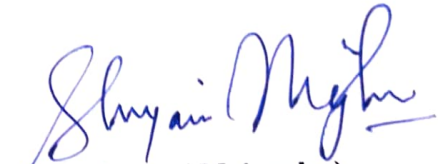
DECLARATION BY THE CANDIDATE

I, **Shreyasi Majumdar**, certify that the work embodied in this Ph.D. thesis is my own bonafide work and carried out by me under the supervision of **Prof. Sairam Krishnamurthy** from **July, 2018 to June, 2024** at the **Department of Pharmaceutical Engineering & Technology, Indian Institute of Technology (Banaras Hindu University), Varanasi**. The matter embodied in this Ph.D. thesis has not been submitted for the award of any other degree/diploma.

I declare that I have faithfully acknowledged and given credit to the research workers wherever their works have been cited in my work in this thesis. I further declare that, I have not willfully copied any other's work, paragraphs, text, data, results, etc. reported in the journals, books, magazines, reports, dissertations, theses, etc., or available at websites and have not included them in this Ph.D. thesis and have not cited as my own work.


Date: 17.3.25

Place: IIT (BHU), Varanasi



(Shreyasi Majumdar)

CERTIFICATE BY THE SUPERVISOR AND HEAD OF THE DEPARTMENT

It is certified that the above statement made by the student is correct to the best of our knowledge.


Prof. Sairam Krishnamurthy
(Supervisor)

Prof. SAIRAM KRISHNAMURTHY
Dept. of Pharm. Engg. & Tech.
Indian Institute of Technology
(Banaras Hindu University)
Varanasi-221005 (U.P.)


Head of the Department
विभागाध्यक्ष / Head
मैद्यकीय अभियांत्रिकी एवं प्रौद्योगिकी विभाग /
Department of Pharmaceutical Engineering & Technology
भारतीय प्रौद्योगिकी संस्थान / INDIAN INSTITUTE OF TECHNOLOGY
(बनारस हिन्दू विश्वविद्यालय) / (BANARAS HINDU UNIVERSITY)
वाराणसी-२२१००५ / Varanasi-221005

COPYRIGHT TRANSFER CERTIFICATE

Title of the Thesis: “Novel calcium-regulating mechanism of barium-doped material for the treatment of neuropathic pain”

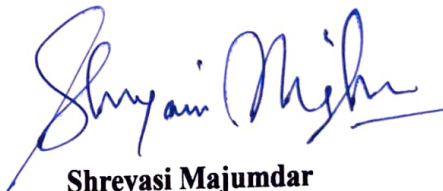
Candidate’s Name: Ms. Shreyasi Majumdar

Copyright Transfer

The undersigned hereby assigns to the Indian Institute of Technology (Banaras Hindu University), Varanasi all rights under copyright that may exist in and for the above thesis submitted for the award of the “*Doctor of Philosophy*”.

Date: 17.3.25

Place: IIT (BHU), Varanasi



Shreyasi Majumdar

Note: However, the author may reproduce or authorize others to reproduce material extracted verbatim from the thesis or derivative of the thesis for author’s personal use provided that the source and University’s copyright notice are indicated.

ACKNOWLEDGEMENTS

This work represents the culmination of years of unwavering dedication, wherein numerous individuals generously extended their support and guidance. Above all, I express my profound gratitude to Lord Shiva for providing me with this remarkable opportunity to express my deepest appreciation to all those who played an instrumental role in assisting and guiding me throughout my research journey. Their unwavering assistance and guidance have been invaluable, and I am truly grateful for their contributions.

At the outset, I would like to pay my tribute to the father and founder of the Banaras Hindu University respected *Mahamana Pt. Madan Mohan Malviya Ji*, because of whom thousands of students every year put their step towards a bright and prosperous future.

I want to express my heartfelt gratitude to my supervisor, *Prof. Sairam Krishnamurthy*, for grooming me not only to conduct independent research but also for acquainting me with other areas affiliated with scientific pursuits. His vast knowledge and logical way of thinking have been of great value to me. This work would not have been possible without his guidance, support and encouragement. His unflinching courage and conviction will always inspire me, and I hope to continue to work with his noble thoughts.

I convey my profound gratitude to my esteemed R.P.E.C members, *Dr. P.K. Nayak* and *Dr. Abha Mishra*, for their invaluable suggestions throughout my Ph.D. tenure.

I am also grateful to *Prof. S. Hemalatha*, Head, Department of Pharmaceutical Engineering & Technology, Indian Institute of Technology (Banaras Hindu University) and *Prof. S.K. Srivastava* (Former Head) for permitting me to utilize the department's resources for my research endeavours.

I want to express my sincere gratitude to all the teachers of the department; *Prof. B. Mishra, Prof. S.K. Singh, Prof. Sanjay Singh, Dr. A.K. Srivastava, Prof. M.S. Muthu, Prof. Senthil Raja, Dr. Alakh N. Sahu, Dr. Ruchi Chawla, Dr. G. P. Modi, Dr. S.K. Mishra, Dr. A. K. Maurya , Dr. Vinod Tiwari, Dr. S. K. Jain, Dr. Rajnish, Dr. A.K.*

Agrawal, Dr. Deepak Kumar, Dr. Dinesh Kumar and Dr. Jairam Meena for their valuable suggestion and guidance throughout the course of my research.

I also want to thank the *Department of Science and Technology* for providing me with financial support through the DST INSPIRE Fellowship.

A special thanks to *Prof. S.K. Trigun* and *Dr. Debasmit Mallick*, from the Department of Zoology, Institute of Science, Banaras Hindu University, India for their help and guidance in molecular analysis.

I wish to express my sincere appreciation to the Sophisticated Analytical & Technical Help Institute (SATHI), Central Discovery Centre (CDC)-BHU, Varanasi, and Central Instrument Facility, IIT (BHU), Varanasi, for their provision of diverse spectroscopic and microscopic techniques utilized in my research work.

It gives me great pleasure to acknowledge the support of my respected seniors and lab mates *Dr. Dhananjay, Dr. Pankaj Paliwal, Dr. Sukesh K. Gupta, Dr. Akanksha Mishra, Dr. Santosh K. Prajapati, Dr. Ramakrishna Kakarla, Dr. Qadir Alam, Dr. Prabha Rajput, Dr. Pratigya Tripathi, Aquib, Gajendra T.A., Neha Singh, Asha, Neeraj, and Swagata* for their stimulating discussion and brilliant suggestions. I would also like to thank my juniors; *Rajesh, Vilas, Shital, Priya, and Kirti* whose moral support always inspired me.

I extend my heartfelt gratitude and indebtedness to my beloved friends *Dr. Poonam Bhadoria and Dr. Parul Rawat* for their affection, love and moral support whenever I was in need.

I pay my sincere thanks to *Mr. Nandlal, Mr. Rafeeq, Mr. Tabrej, Mr. Upadhyay, Mr. Atul Kumar Gupta, Mr. Yashwant Singh, Mr. Anand Kumar, Mr. Jamil, Mr. Virendra*, and all other non-teaching staff of the department for providing all the necessities required for my research.

Most importantly, I would like to express my deepest gratitude to my parents, *Mrs. Ruma Majumdar* and *Mr. Prabir Kumar Majumdar*, for their unwavering blessings, invaluable contributions, and unconditional support at every stage of my life. I am also immensely grateful to my brother, *Pratyaya Majumdar*, for his constant support throughout my journey.

Table of Contents

Certificate	ii
Declaration by the Candidate	iii
Copyright Transfer Certificate	iv
Acknowledgements	v
Table of Contents	vii
List of Tables	xv
List of Figures	xxvii
List of Abbreviations	xxix
Preface	xxxiii
1. Introduction	1
1.1. The Genesis of Idea: From Concept to Cure	1
1.2. The background of bioactive glass	2
1.3. Role of therapeutic ions in soft tissue repair and regeneration	3
1.4. Diverse Applications of Bioactive Glass: Innovations in Medicine and Beyond	5
1.4.1. Bioactive glasses exhibit wound healing property	5
1.4.2. Bioactive glasses facilitate angiogenesis	8
1.4.3. Bioactive glasses in gastrointestinal tissue regeneration	9
1.4.4. Bioactive glasses in myocardial tissue engineering	9
1.4.5. Bioactive glass aids in the peripheral nerve regeneration	10
1.5. Innovation in Biomaterials: The Development of Barium-Doped Bioactive Glass (BaBG)	11
1.6. Understanding Neuropathic Pain: An Introduction	12
1.7. Symptoms of Neuropathic pain	13
1.8. Epidemiology of Neuropathic pain	14
1.9. The physiology of pain perception	15
1.10. Pathophysiology and molecular mechanism of Neuropathic pain	18
1.10.1. Peripheral sensitization:	18
1.10.2. Central sensitization:	20
1.11. Clinical pharmacotherapy for the treatment of Neuropathic pain	23
1.11.1. Calcium channel blockers/ anticonvulsants	23
1.11.2. Nonsteroidal anti-inflammatory drugs (NSAIDs)	24
1.11.3. Antidepressants	25
1.11.4. Opioids	26
1.11.5. Additional pharmacotherapy	27

1.12. Role of ion channels in the development and progression of Neuropathic pain	28
1.12.1. Voltage-Gated Sodium Channels	29
1.12.2. Transient receptor potential (TRP) channels	29
1.12.3. Calcium channels and their role in the development of Neuropathic pain	30
1.13. Role of calcium ions in the pathophysiology of Neuropathic pain	31
1.14. Significance of glial cells in Neuropathic pain	33
1.14.1. Calcium -binding protein: S100 proteins	34
1.14.2. S100 proteins: A key player in the pathophysiology of various diseases	35
1.15. Hypothesis	38
1.16. Objectives:	40
2. Introduction	41
2.1. Materials and Methods	44
2.1.1. Synthesis of the bioactive glasses	44
2.1.1.1. Barium doped Bioactive glass (BaBG)	44
2.1.1.2. 45S5	45
2.1.2. Characterization of the bioactive glass samples	45
2.1.2.1. Particle size and surface area determination	45
2.1.2.2. X-Ray Diffraction (XRD)	46
2.1.2.3. Fourier Transform Infrared (FTIR) Spectroscopy	46
2.1.2.4. Transmission electron microscopy (TEM)	47
2.1.3. Preparation of SBF (Simulated Body Fluid)	47
2.1.4. pH behavior of 45S5 and BaBG in SBF	47
2.1.5. In vitro hydroxyapatite forming ability of BaBG and 45S5	47
2.1.6. Surface characterization and quantitative elemental analysis of BaBG and 45S5	48
2.1.7. Hemolysis assay	48
2.1.8. Cell line and cell culture	49
2.1.9. In vitro cytotoxicity assay	49
2.1.10. Apoptosis assay (AO/EtBr)	50
2.1.11. In vitro cell growth/proliferation assay	50
2.1.12. Scratch-wound healing assay	51
2.1.13. Evaluation of the anti-inflammatory activity of bioactive glasses against LPS-induced inflammation	51
2.1.14. Data Analysis	52
2.2. Results and Discussion	52

2.2.1. Particle size and surface area analysis	52
2.2.2. X-ray diffraction (XRD) analysis of BaBG & 45S5	53
2.2.3. FTIR analysis of the bioactive glasses	56
2.2.4. Transmission electron microscopy (TEM) analysis	58
2.2.5. pH behavior of the bioactive glass samples in the SBF solution	58
2.2.5. SEM and EDX analysis of BaBG and 45S5	62
2.2.6. BaBG and 45S5 shows biocompatibility in hemolysis assay	64
2.2.7. BaBG and 45S5 exhibit cytocompatibility during in vitro cell proliferation and cytotoxicity assay	65
2.2.8. BaBG and 45S5 exhibits cytocompatibility during acridine orange/ethidium bromide staining	68
2.2.9. BaBG and 45S5 shows regeneration during the scratch assay	70
2.2.10. BaBG and 45S5 exhibits anti-inflammatory properties	72
2.3. Conclusion	74
3. Introduction	76
3.1. Materials and Methods	78
3.1.1. Materials	78
3.1.2. Preparation of Simulated body fluid (SBF)	78
3.1.3. <i>In vitro</i> pharmacokinetic study of BaBG	78
3.1.4. Animals	79
3.1.5. Experimental design for single dose oral in-vivo pharmacokinetic study	79
3.1.6. Pharmacokinetic Analysis	80
3.1.7. Analysis of Ca, Si, and Ba in urine and feces	81
3.1.8. Experimental design for in-vivo biodistribution study after single dose oral administration of BaBG	81
3.1.9. Scanning electron microscopy (SEM) of vital organs	82
3.1.10. Digestion of the biological samples for ICP-MS	82
3.1.11. Inductively coupled plasma-mass spectroscopy (ICP-MS)	83
3.1.12. Body weight and organ coefficient	84
3.1.13. Statistical analysis	84
3.2. Results and discussion	84
3.2.1. Temporal <i>in vitro</i> release of Ca, Si, and Ba from BaBG in SBF solution	84
3.2.2. <i>In vivo</i> oral pharmacokinetic study	87
3.2.2.1. The plasma concentration of Ca, Ba, and Si released from BaBG in rats during the <i>in vivo</i> pharmacokinetic study	87

3.2.2.2. <i>In vivo</i> oral pharmacokinetic profile of Ca, Ba, and Si released from BaBG	91
3.2.3. Urinary and fecal excretion	95
3.2.4. Changes in body weight and organ coefficient after oral administration of BaBG	100
3.2.5. <i>In vivo</i> biodistribution of Ca, Ba, and Si in vital organs and their scanning electron microscopical analysis	100
3.3. Summary	107
4. Introduction	108
4.1. Materials and Methods	109
4.1.1. Materials	109
4.1.2. Animals	109
4.1.3. Acute oral toxicity study	110
4.1.4. Subacute oral toxicity study	111
4.1.5. Behavioral assessments	112
4.1.5.1. Rotarod test	112
4.1.5.2. Open field test (OFT)	113
4.1.5.3. Grip strength test	114
4.1.5.4. Spontaneous locomotor activity (Actophotometer)	114
4.1.6. Organ coefficient	114
4.1.7. Preclinical pathology	115
4.1.8. Hematology	115
4.1.9. Biochemical analysis	115
4.1.10. Histological analysis	116
4.1.11. Statistical analysis	116
4.2. Results and discussion	116
4.2.1. Acute toxicity study	116
4.2.1.1. General observation and behavioral analysis	116
4.2.1.2. Effect of BaBG on the body weight during the acute toxicity study	118
4.2.1.3. Effect of BaBG on the organ coefficient during the acute toxicity study	119
4.2.1.4. Effect of BaBG on various enzymes during the acute toxicity study	121
4.2.1.5. Histological analysis of various organs of BaBG-treated rats during the acute toxicity study	124
4.2.2. Sub-acute toxicity study	129
4.2.2.1. General observations	129

4.2.2.2. Effect of BaBG on the body weight and food consumption during the sub-acute toxicity study	131
4.2.2.3. Effect of BaBG on hematological parameter during the sub-acute toxicity study	132
4.2.2.4. Effect of BaBG on organ-coefficient during the sub-acute toxicity study	132
4.2.2.5. Effect of BaBG on various enzymes during the sub-acute toxicity study	134
4.2.2.6. Effect of BaBG on the neurobehavioral activity during sub-acute toxicity study	137
4.2.3.7. Histological analysis of various organs of BaBG treated rats during the sub-acute toxicity study	139
4.3. Summary	148
5. Introduction	149
5.1. Materials and methods	154
5.1.1. Materials	154
5.1.2. Experimental animals and their ethical statement	154
5.1.3. Chronic constriction injury (CCI) model of Neuropathic pain	155
5.1.4.1. Animal experimental design for the temporal study to measure the changes in the intercellular calcium (Ca^{2+}) _i and S100b level	156
5.1.4.2. Animal experimental design for validation of the role of S100b in the pathogenesis/progression of NP	157
5.1.5. Behavioral analysis:	159
5.1.5.1. Thermal hyperalgesia (hot-plate test)	159
5.1.5.2. Cold allodynia (acetone drop test)	159
5.1.5.3. Mechanical hyperalgesia (Randall Selitto test)	159
5.1.5.4. Dynamic mechanical allodynia (Cotton swab test)	160
5.1.5.5. Rota rod	160
5.1.5.6. Sciatic functional index (SFI)	161
5.1.5.7. BBB (Basso, Beattie, and Bresnahan) locomotor test	161
5.1.6. Gastrocnemius muscle mass assessment	162
5.1.7. Real Time quantitative PCR	162
5.1.8. Assessment of S100b, TNF- α , and IL-6 protein level in sciatic nerve and spinal cord	165
5.1.9. Immunofluorescence	165
5.1.10. Golgi–Cox Staining	166
5.1.10.1. General Precautions	166
5.1.10.2. Preparation of Solutions	166

5.1.10.3. Procedure for staining	167
5.1.10.4. Quantification of dendritic branching and spine density	168
5.1.11. Measurement of intracellular calcium level	169
5.1.12. Histological analysis of gastrocnemius muscle	169
5.1.13. Statistical analysis	169
5.2. Results and Discussion	170
5.2.1. Temporal study to evaluate the development of NP phenotypes and changes in the intracellular calcium and S100b protein level	170
5.2.1.1. Effect of CCI on the development of NP phenotypes during the temporal study	170
5.2.1.2. Temporal changes in the intracellular calcium, S100b, and pro-inflammatory cytokine (TNF- α) level post-CCI of sciatic nerve	172
5.2.2. Validation of the role of S100b in the pathogenesis/progression of NP in rat CCI model	176
5.2.2.1. Effect of pentamidine on the CCI-induced sensory and motor deficits	176
5.2.2.2. Effect of pentamidine on the CCI-induced motor coordination	179
5.2.2.3. Effect of pentamidine on the intracellular calcium (Ca^{2+}) _i and S100b level in SN and SC	181
5.2.2.4. Effect of pentamidine on the $\text{Ca}_v2.2$ and TRPV1 mRNA expression in SN and SC	184
5.2.2.5. Effect of pentamidine on the expression of S100b in SN and SC	186
5.2.2.6. Effect of pentamidine on the CCI-induced microglial activation in SN and SC	187
5.2.2.7. Effect of pentamidine on the CCI-induced astrocytes activation in SN and SC	188
5.2.2.8. Effect of pentamidine on the CCI-induced neuroinflammation	192
5.2.2.9. Effect of pentamidine on the neuronal morphology post-CCI injury	193
5.2.2.10. Effect of pentamidine on the gastrocnemius muscle post-CCI injury	196
5.2.2.11. Effect of pentamidine on the gastrocnemius muscle post-CCI injury	197
5.3. Conclusion	199

6. Introduction	202
6.1. Materials and methods	207
6.1.1. Materials	207
6.1.2. Experimental animals and their ethical statement	207
6.1.3. <i>Ex vivo</i> electrophysiological assessment of calcium channel blocking effects of BaBG	208
6.1.3.1. Preparation of physiological fluid (PF)	208
6.1.3.2. <i>Ex vivo</i> electrophysiological assessment	208
6.1.4. Chronic constriction injury (CCI) model of Neuropathic pain	210
6.1.5. Experimental design for pharmacological evaluation of BaBG for the treatment of NP	210
6.1.6. Behavioral analysis:	212
6.1.6.1. Thermal hyperalgesia (hot-plate test)	212
6.1.6.2. Cold allodynia (acetone drop test)	212
6.1.6.3. Mechanical hyperalgesia (Randall Selitto test)	213
6.1.6.4. Dynamic mechanical allodynia (Cotton swab test)	213
6.1.6.5. Rota rod	213
6.1.6.6. Sciatic functional index (SFI)	214
6.1.6.7. BBB (Basso, Beattie, and Bresnahan) locomotor test	215
6.1.7. Electrophysiological measurement of action potential	215
6.1.8. Electromyogram (EMG) recordings	216
6.1.9. Gastrocnemius muscle mass assessment	217
6.1.10. Real Time quantitative PCR	217
6.1.11. Assessment of S100b, TNF- α , IL-6, and IL-10 protein level in sciatic nerve and spinal cord	218
6.1.12. Immunofluorescence analysis	218
6.1.13. Golgi–Cox Staining	218
6.1.14. Measurement of intracellular calcium level	218
6.1.15. Histological analysis of gastrocnemius muscle	218
6.1.16. Histological analysis of sciatic nerve (SN) using luxol fast blue staining	219
6.1.17. In silico docking of S100b proteins with metal ions (Ca ²⁺ and Ba ²⁺)	219
6.1.17.1. Preparation of Ligand and Protein	219
6.1.17.2. Analysis and Visualization	220
6.1.18. Statistical analysis	220
6.2. Results and Discussion	220

6.2.1. Effect of calcium channel blocking (CCB) properties of BaBG in the <i>ex vivo</i> setup	220
6.2.2. Effect of BaBG on mechanical /thermal hyperalgesia and allodynia	226
6.2.3. Effect of BaBG on the CCI-induced alterations in motor functions	228
6.2.4. Effect of BaBG on the mRNA expression of TRPV1 and CaV 2.2 along with the intracellular calcium level (Ca^{2+}) _i in the SN and SC post-CCI	231
6.2.5. Effect of BaBG on the expression of S100b in SN and SC	234
6.2.6. Effect of BaBG on the CCI-induced astrocytes activation in SN and SC	237
6.2.7. Effect of BaBG on the CCI-induced neuroinflammation	239
6.2.8. Effect of BaBG on the neuronal morphology post-CCI injury	244
6.2.9. Effect of BaBG on the CCI-induced axonal degeneration	247
6.2.10. Effect of BaBG on the electrophysiological response upon stimulating the sciatic nerve	250
6.2.11. Effect of BaBG on the muscle functioning in response to the cold-stimulus-evoked allodynia	251
6.2.12. Effect of BaBG on the gastrocnemius muscle post-CCI injury	252
6.3. Conclusion	255
7. Summary and Conclusion	258
7.1. Important outcomes	262
7.2. Scope for Further Work	263
Bibliography	264
List of Publications	289

LIST OF FIGURES

Figure 1.1	The primary afferent pathways and its connections in the dorsal horn of spinal cord	17
Figure 1.2	The ascending pathway of the pain perception	18
Figure 1.3	The peripheral changes in the primary afferent neuron after the peripheral nerve injury	20
Figure 1.4	The mechanisms of central sensitization of WDR neurons. Diagram showing the various mechanisms involved in neuropathic pain at different sites in the nociceptive pathway	22
Figure 1.5	The proposed hypothesis of pharmacological evaluation of BaBG in the experimental model of neuropathic pain	38
Figure 2.1	Nitrogen adsorption-desorption isotherm of (A) 45S5 and (B) BaBG at STP (standard temperature and pressure)	53
Figure 2.2	XRD pattern of BaBG & 45S5 bioactive glass samples before SBF treatment (A) and XRD pattern of 45S5 (B) and BaBG (C) after soaking them in SBF for 1, 3, 7, and 14days	58
Figure 2.3	FTIR transmittance spectra of the bioactive glasses before soaking it in SBF solution (A) and FTIR spectra of 45S5 (B) and BaBG (C) after immersion in the SBF solution for 1, 3, 7, and 14 days	60
Figure 2.4	The morphology and phase analysis of the synthesized BaBG and 45S5. (A) TEM image and (B) SAED pattern of 45S5 and BaBG	61
Figure 2.5	The changes in the pH of the SBF solution after soaking BaBG and 45S5 for 30 days	61
Figure 2.6	SEM micrographs of (i) 45S5 (A) and BaBG (B) before immersion in SBF, (ii) 45S5 and (iii) BaBG after the SBF treatment for 1 (A), 3 (B), and 14 (C) days respectively	63
Figure 2.7	EDX analysis of (i) 45S5 and (ii) BaBG after 1 (A) and 14 (B) days of SBF treatment	64
Figure 2.8	Effect of BaBG & 45S5 sample on hemolysis at different concentrations (i) and micrographs of RBC cells after incubation with negative control (A), positive control (B), 45S5 (C) and BaBG (D) respectively. All values are mean \pm SD (n=4). ^a p<0.05, ^b p<0.05, ^c p<0.05 and ^d p<0.05 compared to 5, 10.25 and 50 mg respectively. (Two-way ANOVA followed by Bonferroni post hoc test)	67
Figure 2.9	Effect of BaBG & 45S5 on percentage proliferation (A), percentage cytotoxicity of K562 cells at different concentrations (B) and percentage cell proliferation of the C6 cells at various time intervals (C). All values are mean \pm SD (n=4). ^a P<0.05, ^b P<0.05, ^c p<0.05 and ^d p<0.05 compared to 5, 10, 25 and 50 μ g/ml of bioactive glass sample (BaBG and 45S5), ^x p<0.05, ^y p<0.05 compared to 24 and 48 h of	69

	incubation with BaBG and 45S5 and ^s p<0.05 and [@] p<0.05 compared to control (culture medium treated) and 45S5 treated group (Two-way ANOVA followed by Bonferroni post hoc test)	
Figure 2.10	Apoptosis assay of C6 cells following treatment with BaBG (A) and 45S5 (B) with Acridine orange/ Ethidium bromide. Green color staining with Acridine orange suggests the living and healthy cells and the Ethidium bromide is staining for nucleic acid. Bright-field (i), Acridine orange staining (ii), Ethidium bromide staining (iii), the merge of ii over iii (iv), overlay of iv over i (v). Arrow indicates early apoptotic cells	70
Figure 2.11	Scratch/wound healing assay in C6 cells following treatment with BaBG, 45S5, or Temozolomide (TMZ) (A), time-dependent percentage wound recovery in C6 cells treated with the above formulations (B) and comparison of time-dependent percent wound area recovery to wound area created in the presence of culture medium, BaBG, 45S5 or TMZ (C-F). All values are mean ± SD (n=3). ^a P<0.05, ^b P<0.05 and ^c p<0.05, compared to culture media, 45S5 and BaBG treatment and [@] p<0.05, [#] p<0.05 and ^s p<0.05 compared to 4, 8 and 16 h of incubation of C6 cells (Two-way ANOVA followed by Bonferroni post hoc test)	72
Figure 2.12	Effect of BaBG and 45S5 on IL-6 (A), TNF-α (B) and IL-10 (C) level in C6 cells. All values are mean ± SD (n=3). ^a P<0.05, ^b P<0.05 and ^χ p<0.05 compared to vehicle (culture media treated), LPS, and 45S5 treatment groups (Two-way ANOVA followed by Bonferroni post hoc test)	74
Figure 3.1	Schematic representation of the experimental protocol of the in-vivo single-dose oral pharmacokinetics study of BaBG	80
Figure 3.2	Schematic representation of the experimental protocol of the in-vivo biodistribution study after single-dose oral administration of BaBG	82
Figure 3.3	The release pattern of Ca (A), Si (B), and Ba (C) in SBF solution at pH 7.4 from BaBG at various time intervals for 7 days using ICP-MS and their representation by heatmap(D)	86
Figure 3.4	Plasma concentration profile of Ca (i), Ba (ii), and Si (iii) released from BaBG administered orally with the heatmap representation of the plasma concentration of Ca, Ba, and Si (iv). All values are in mean ± SD (n=7 rats/ group). [@] p<0.05, ^a p<0.05, and ^b p<0.05 compared to control, dose 1mg/kg and 5 mg/kg of BaBG respectively. ^w p<0.05, ^x p<0.05, and ^y p<0.05 compared to 1, 24, 48 h respectively (Two-way ANOVA followed by Bonferroni post-hoc test)	90-91
Figure 3.5	Representative scanning electron microscopy image of the stomach of the control and BaBG-treated rat exhibiting the deposition of abundant hydroxyapatite (HA) crystals on the gastric epithelium layer of the stomach without any abrasion	106

of the protective layer qualitatively. The macroscopic photographs of the stomach of both the groups are also showing normal morphology. Magnification: 5k X; scale bars: 2 μ m

- Figure 3.6 Representative photograph of the scanning electron microscopy of liver (i), spleen (ii), kidney (iii), heart (iv), lungs (v), and brain (vi) section of control (A) and orally treated BaBG rat (B). The liver section of the treated rat exhibited the presence of normal hepatocytes (H) surrounding the sinusoids (S) and central vein (CV). The deposition of hydroxyapatite (HA) along with the presence of erythrocytes (RBC; shown in red arrow) is seen. The spleen of BaBG-treated rat exhibiting abundant hydroxyapatite (HA) deposition and the lungs of control and BaBG rats also exhibited normal alveoli (A) and alveolar duct (Ad). Similarly, the cross-section of the kidneys of treated rat exhibited normal architecture of the Bowman's capsule (B; yellow arrow) along with the glomerular tuft. There are also podocytes (P) and erythrocytes (RBC) visible along with the deposition of crystals of HA. The SEM analysis of heart exhibited intact myofibres (Myo) with the presence of loose connective tissue and collagen fibers (CF). BaBG rats exhibited normal surface morphology in brain section similar to the control rats without any deposition of HA. Magnification of liver, spleen, lung, and heart: 550X and 5 kX; scale bars: 40 μ m and 4 μ m respectively. Magnification of kidneys: 450 X and 1.5 kX; scale bars: 50 μ m and 10 μ m respectively. Magnification of brain: 1 kX and 5 kX; scale bars: 20 μ m and 4 μ m respectively 106
- Figure 4.1 Schematic representation of the experimental protocol for single-dose acute toxicity study (OECD 423) to determine the LD50 cut-off (mg/kg b.w.) value. The starting dose of 300 mg/kg b.w. was selected. If 2-3 animals die, a lower test dose (i.e., 50 mg/kg) was tested and if no or one animal dies, the next higher dose (i.e., 2000 mg/kg) was tested. Black arrow indicates the test procedure followed in our study 111
- Figure 4.2 Schematic representation of the repeated 28-day oral toxicity study as per OECD 407 guidelines. In the subacute toxicity study, rats (n=10/group) were administered BaBG (dose: 50, 500, and 1000 mg/kg b.w.) and were observed daily for any sign of toxicity 113
- Figure 4.3 Representative macroscopic photographs showing normal morphology of (i) 45S5 [liver (A), brain (B), kidneys (C), spleen (D), and lungs (E)] and (ii) BaBG [liver (F), brain (G), kidneys (H), spleen (I), and lungs (J)] treated rats after single-dose administration of highest dose (i.e., 2000 mg/kg b.w.) at the end of day 14 118

Figure 4.4	Effect of single-dose oral administration of BaBG and 45S5 on body weight of rats at various time points during the experimental protocol. All values are in mean \pm SD (n=6 female rats/ group). (Two-way ANOVA followed by Bonferroni post hoc test)	119
Figure 4.5	Effect of single-dose oral administration of BaBG and 45S5 on organ coefficient of the brain (A), heart (B), lung (C), kidneys (D), liver (E), and spleen (F) at the end of the experimental protocol. All values are in mean \pm SD (n=6 female rats/ group). (One-way ANOVA followed by Tukey's multiple comparison post hoc test)	121
Figure 4.6	Effect of single-dose oral administration of BaBG and 45S5 on serum concentration of AST (A), ALT (B), ALP (C), creatinine (D), CK-MB (E), and calcium (F) at the end of the experimental protocol. All values are in mean \pm SD (n=6 female rats/ group). (One-way ANOVA followed by Tukey's multiple comparison post hoc test)	126
Figure 4.7	Effect of single-dose oral administration of BaBG and 45S5 (dose of 300 and 2000 mg/kg b.w.) on highly perfused organs like brain, heart, lung, liver, kidney, and spleen tissue stained with hematoxylin and eosin	129
Figure 4.8	Effect of repeated-dose 28 days oral administration of BaBG and 45S5 (50, 500, and 1000 mg/kg) on body weight of male (A) and female (C) rats along with their food intake (B and D, respectively) during the experimental protocol. All values are in mean \pm SD (n=5 rats/ group). (Two-way ANOVA followed by Bonferroni post -hoc test)	131
Figure 4.9	Schematic representation of the track plot of (i) male and (ii) female rats respectively divided into following groups: control (A), 45S5 (B, C, D; dose: 50, 500, and 1000 mg/kg b.w. respectively), and BaBG (E, F, G; dose: 50, 500, and 1000 mg/kg b.w. respectively) recorded during 5 min test sessions on day 28 (ANYMAZE)	139
Figure 4.10	Histological analyses of the brain tissue of control (A), 45S5, and BaBG (B and C respectively; dose: 1000 mg/kg b.w.) treated male and female rats after repeated 28 days oral administration. Bar: 50 μ m and 20 μ m. Hematoxylin and eosin staining	142
Figure 4.11	Histological analyses of the lungs of control (A), 45S5, and BaBG (B and C respectively; dose: 1000 mg/kg b.w.) treated male and female rats in subacute toxicity study. 45S5 and BaBG treated rats exhibited normal appearance of alveoli with thin epithelial walls surrounded by capillaries similar to the control rats. Edema or alveolar hemorrhage in the alveolar cavities was also not observed in the treatment groups. Bar: 100 μ m. Hematoxylin and eosin staining	143

- Figure 4.12 Histological analyses of the heart of control (A), 45S5, and BaBG (B and C respectively; dose: 1000 mg/kg b.w.) treated male and female rats. The heart of 45S5 and BaBG treated rats exhibited normal morphology with oval and centrally located nuclei in cardiomyocytes regularly arranged in myofibres. No vacuolar degeneration of the myofibrils was observed in 45S5 and BaBG rats. Bar: 50 μ m. Hematoxylin and eosin staining 144
- Figure 4.13 Effect of repeated-dose 28 day oral administration of BaBG and 45S5 on microstructure of liver (dose: 1000 mg/kg b.w.) in male and female rats. (A) Control and (B) 45S5 treated male and female rats exhibited normal hepatocytes with intact vesicular nucleus radiating from the central vein surrounding the portal tract. No congestion of the central vein or dilation of the sinusoid was observed. (C) The female BaBG treated rats showed mild lymphoid infiltration in the portal areas without any sinusoid dilation. Bar: 100 μ m. Hematoxylin and eosin staining 145
- Figure 4.14 Effect of repeated-dose 28 day oral administration of BaBG and 45S5 on microstructures of kidney (dose: 1000 mg/kg b.w.) in male and female rats. The cross-section of (A) control, (B) 45S5, and (C) BaBG treated male and female rats exhibited normal architecture of glomeruli, bowman's capsule, and renal corpuscles with intact proximal and distal convoluted tubules. Bar: 50 μ m. Hematoxylin and eosin staining 146
- Figure 4.15 Effect of repeated-dose oral administration of BaBG and 45S5 (dose: 1000 mg/kg b.w.) on spleen of male and female rats. The cross-section of (A) control, (B) 45S5, and (C) BaBG treated male and female rats showed normal appearance of the lymphatic nodules of white pulp, splenic cords of red pulp, and the spleen trabecula. Bar: 50 μ m. Hematoxylin and eosin staining 147
- Figure 5.1 Presents a graphical representation depicting the schematic diagram outlining the proposed hypothesis concerning the molecular mechanism underlying the pathogenesis of NP in a CCI-induced NP rat model. The injury to the sciatic nerve (SN) leads to the development of central sensitization due to upregulation in the expression of calcium channels (Cav2.2) in the dorsal horn of spinal cord (SC). Besides, there are also enhanced expression of heat-sensing TRPV1 channels in the SC. Upregulation in the expression of these channel results increase in the influx of calcium ions leading to hyperexcitation of the nociceptive neurons and development of NP phenotypes. In addition, the resident immune cells of CNS i.e., glial cells (astrocytes and microglia) get activated post-CCI leading to increase in release of calcium-binding 153

proteins i.e., S100b. S100b gets activated in presence of calcium ions causing release of pro-inflammatory cytokines and progression of NP. Therefore, the temporal changes in the intracellular calcium and S100b protein level will help to identify the pharmacological window of opportunity. Besides, to validate the role of S100b in the pathogenesis and progression of NP in this model, we have used specific S100b inhibitor i.e., pentamidine to evaluate its effect on NP phenotypes

- Figure 5.2 Schematic representation of the experimental protocol followed for the CCI-induced neuropathic pain model and the behavioral assessment of the symptoms developed post-surgery 156
- Figure 5.3 Schematic representation of the experimental protocol followed for the temporal study performed to measure the intracellular calcium and S100b level in the CCI-induced neuropathic pain model 157
- Figure 5.4 Schematic representation of the experimental protocol followed for validation of the role of S100b in the pathogenesis/progression of NP in the CCI-induced NP model in rats 158
- Figure 5.5 Sensory and motor deficit due to chronic constriction injury in rats. The effect of CCI on the development of (A) thermal hyperalgesia, (B) cold allodynia, (C) mechanical hyperalgesia, and (D) changes in the BBB score. All values are in mean \pm SD (n=4 rats/ group). ^ap<0.05, ^bp<0.05, and ^cp<0.05 compared to D-0, D-3, and D-7 respectively. (One-way ANOVA followed by Tukey multiple comparison post-hoc test) 172
- Figure 5.6 Temporal changes in the intracellular calcium, S100b and TNF- α level in SN and SC post-CCI injury. All values are in mean \pm SD (n=4 rats/ group). ^ap<0.05, ^bp<0.05, ^cp<0.05, ^dp<0.05, ^ep<0.05, and ^fp<0.05 compared to 0, 0.25, 0.5, 1, 3, and 7 days post-injury. (One-way ANOVA followed by Tukey's multiple comparison post-hoc test) 175
- Figure 5.7 (A) A correlation between intracellular calcium level, S100b, and TNF- α level on D-21 post-CCI. (B) A correlation between S100b level and NP phenotypes on D-21 post-CCI 175
- Figure 5.7 (B) A correlation between S100b level and NP phenotypes on D-21 post-CCI of peripheral nerve. 176
- Figure 5.8 Sensory and motor deficit due to chronic constriction injury in rats. Effect of pentamidine on (A) thermal hyperalgesia, (B) cold allodynia, (C) mechanical hyperalgesia, (D) dynamic mechanical allodynia, and (E) retention time on the rota-rod. All values are in mean \pm SD (n=12 rats/ group). ^ap<0.05, ^bp<0.05, ^cp<0.05, and ^dp<0.05 compared to control, sham, CCI, and pentamidine respectively. (Two-way ANOVA followed by Bonferroni post-hoc test) 179

Figure 5.9	Representative images of the (i) paw of the ipsilateral side and (ii) footprints of control, CCI, pentamidine and pregabalin treated rats. (ii) Effect of pentamidine on SFI and BBB score. All values are in mean \pm SD (n=12 rats/ group). ^a p<0.05, ^b p<0.05, ^c p<0.05, and ^d p<0.05 compared to control, sham, CCI, and pentamidine respectively. (Two-way ANOVA followed by Bonferroni post-hoc test)	181
Figure 5.10	Effect of pentamidine on (i) intracellular calcium and (ii) S100b level in SN and SC. All values are in mean \pm SD (n=4 rats/ group). ^a p<0.05, ^b p<0.05, ^c p<0.05, and ^d p<0.05 compared to control, sham, CCI, and pentamidine respectively. (Two-way ANOVA followed by Bonferroni post-hoc test for Fura 2-AM assay) (One-way ANOVA followed by Tukey's multiple comparison post-hoc tests for S100b level)	183
Figure 5.11	A correlation between S100b and NP phenotypes after the pentamidine treatment (10mg/kg b.w.)	183
Figure 5.12	Effect of pentamidine on Cav2.2 and TRPV1 mRNA expression in the SN (A and C respectively) and SC (B and D respectively). All values are in mean \pm SD (n=4 rats/ group). ^a p<0.05, ^b p<0.05, ^c p<0.05, and ^d p<0.05 compared to control, sham, CCI, and pentamidine respectively. (One-way ANOVA followed by Tukey's multiple comparison post-hoc test)	186
Figure 5.13	Effect of pentamidine on S100b expression in the SN. Scale bar was set at 50 μ M with 20X magnification. All values are in mean \pm SD (n=3 rats/ group). ^a p<0.05, ^b p<0.05, ^c p<0.05, and ^d p<0.05 compared to control, sham, CCI, and pentamidine respectively. (One-way ANOVA followed by Tukey's multiple comparison post-hoc test)	189
Figure 5.14	Effect of pentamidine on S100b expression in the SC. Scale bar was set at 50 μ M with 20X magnification. All values are in mean \pm SD (n=3 rats/ group). ^a p<0.05, ^b p<0.05, ^c p<0.05, and ^d p<0.05 compared to control, sham, CCI, and pentamidine respectively. (One-way ANOVA followed by Tukey's multiple comparison post-hoc test)	190
Figure 5.15	Effect of pentamidine on Iba-1 expression in the SC. Scale bar was set at 50 μ M with 20X magnification. All values are in mean \pm SD (n=3 rats/ group). ^a p<0.05, ^b p<0.05, and ^c p<0.05 compared to control, sham, and CCI respectively. (One-way ANOVA followed by Tukey's multiple comparison post-hoc test)	190
Figure 5.16	Effect of pentamidine on GFAP expression in the SN. Scale bar was set at 50 μ M with 20X magnification. All values are in mean \pm SD (n=3 rats/ group). ^a p<0.05, ^b p<0.05, and ^c p<0.05 compared to control, sham, and CCI respectively. (One-way ANOVA followed by Tukey's multiple comparison post-hoc test)	191

Figure 5.17	Effect of pentamidine on GFAP expression in the SC. Scale bar was set at 50 μ M with 20X magnification. All values are in mean \pm SD (n=3 rats/ group). ^a p<0.05, ^b p<0.05, and ^c p<0.05 compared to control, sham, and CCI respectively. (One-way ANOVA followed by Tukey's multiple comparison post-hoc test)	191
Figure 5.18	Effect of pentamidine on (i) NF- κ B mRNA expression and (ii) TNF- α and IL-6 levels in the SN and SC. All values are in mean \pm SD (n=4 rats/ group). ^a p<0.05, ^b p<0.05, ^c p<0.05, and ^d p<0.05 compared to control, sham, CCI, and pentamidine respectively. (One-way ANOVA followed by Tukey's multiple comparison post-hoc test)	193
Figure 5.19	Representative images of Golgi-cox impregnated spinal cord slice of control, sham, CCI, pentamidine, and pregabalin treated rats. Scale bar was set at 200, 100, and 50 μ M	195
Figure 5.20	(i) Representative image of the camera lucida drawing of neuron of SC which is superimposed over concentric circles using Sholl analysis. (ii) Effect of pentamidine on (A) number of branching points across the soma, (B) dendrite length at radial distance from the soma and (C) the total length of dendrites. All values are in mean \pm SD (n=4 / group). ^a p<0.05 and ^b p<0.05 compared to control and sham respectively. (One-way ANOVA followed by Tukey's multiple comparison post-hoc test)	195
Figure 5.21	Effect of pentamidine on NF-L expression in the SN. Scale bar was set at 50 μ M with 20X magnification. All values are in mean \pm SD (n=3 rats/ group). ^a p<0.05, ^b p<0.05, and ^c p<0.05 compared to control, sham, and CCI respectively. (One-way ANOVA followed by Tukey's post-hoc test)	198
Figure 5.22	(A) Representative images of the gastrocnemius muscle of the contralateral and ipsilateral side of the leg. (B) Representative image of the histological analyses of gastrocnemius muscle stained with hematoxylin and eosin at the end of 21st day post-surgery. (C and D) Effect of pentamidine on gastrocnemius muscle weight and cross-section area of muscle fiber. All values are in mean \pm SD (n=5 rats/ group). ^a p<0.05, ^b p<0.05, ^c p<0.05, and ^d p<0.05 compared to control, sham, CCI, and pentamidine respectively. (One-way ANOVA followed by Tukey's multiple comparison post-hoc test)	199
Figure 5.23	Showcases the specific objective's outcome in exploring the molecular mechanism behind neuropathic pain (NP) in a CCI-induced rat NP model. It suggests that the development and progression of NP is associated temporal increase in the intracellular calcium and calcium-binding protein i.e., S100b. Treatment with pentamidine, a specific S100B inhibitor, significantly reversed the neuropathic pain phenotypes induced by CCI. Besides, CCI of peripheral nerve caused	201

hyperactivation of astrocytes and microglia that was induced by S100B and pentamidine attenuated these observed changes. Treatment with pentamidine also lowered the S100B-induced increase in pro-inflammatory markers, specifically TNF- α and IL-6, in both the SC and SN post-injury. Therefore, these findings highlight that S100b is involved in progression and development of NP phenotypes in the CCI-induced NP model and could be the essential factor for an analgesic drug for better management of NP

- Figure 6.1 Presents a graphical representation depicting the schematic diagram outlining the proposed hypothesis concerning the molecular mechanism underlying the pathogenesis of NP in a CCI-induced NP rat model. The injury to the sciatic nerve (SN) leads to central sensitization due to upregulation in the expression of calcium channels (*Cav2.2*) in the dorsal horn of spinal cord (SC). Besides, there are also enhanced expression of heat-sensing TRPV1 channels in the SC. Enhanced expression of these channel results increase in the influx of calcium ions leading to hyperexcitation of the nociceptive neurons and development of NP phenotypes. In addition, the glial cells get activated post-CCI leading to increase in release of calcium-binding proteins i.e., S100b that further triggers the release of pro-inflammatory cytokines and contributes to the progression of NP. Barium-doped bioactive glass (BaBG) leaches barium ion from its framework after coming in contact with the physiological fluid. BaBG, due to its calcium modulating effects may alleviate sensory and motor deficits observed in the CCI-induced NP in rats. It may also prevent the activation of calcium-binding protein i.e., S100b, reduce neuroinflammation, and concurrently cause axonal repair and remodelling; hence may have disease modifying effects 206
- Figure 6.2 Schematic representation of the Plexiglas nerve bath chamber nerve apparatus with the ground, stimulating, and recording electrode used in the experiment. The isolated sciatic nerve (SN) is placed over the platform of nerve chamber in presence of physiological fluid containing the test compounds is stimulated and the compound nerve action potential (CAP) generated is recorded 209
- Figure 6.3 Schematic representation of the experimental protocol followed for the pharmacological evaluation of BaBG for the treatment of NP in rat CCI model 211
- Figure 6.4 Representative images of the EMG recording from the gastrocnemius muscle in response to the cold-stimulus-evoked allodynia in the experimental rats 216
- Figure 6.5 Effect of BaBG on the generation of CAP. All values are mean \pm SD (n=4). ^ap<0.05, ^bp<0.05, ^cp<0.05, ^dp<0.05, ^ep<0.05, and ^fp<0.05 compared to groups i.e., in the PF, in the PF containing 224-225

- Pregabalin, in the PF containing BaBG, in the PF containing BaCl₂, in the PF containing 45S5, in the PF containing reduced calcium ions and BaBG, and in the PF containing BaBG and Pregabalin respectively. (One-way ANOVA followed by Tukey's post hoc test)
- Figure 6.6 Effect of BaBG on (A) mechanical hyperalgesia, (B) thermal hyperalgesia, (C) cold allodynia, and (D) dynamic mechanical allodynia. All values are in mean \pm SD (n=12 rats/ group). ^ap<0.05, ^bp<0.05, ^cp<0.05, ^dp<0.05, ^ep<0.05, and ^fp<0.05 compared to control, CCI, BaBG-1, BaBG-5, BaBG-10, and 45S5-10 respectively (Two-way ANOVA followed by Bonferroni post-hoc test) 228
- Figure 6.7 Effect of BaBG on (A) SFI, (B) BBB score, and (C) time spent on rota rod. All values are in mean \pm SD (n=12 rats/ group). ^ap<0.05, ^bp<0.05, ^cp<0.05, ^dp<0.05, ^ep<0.05, and ^fp<0.05 compared to control, CCI, BaBG-1, BaBG-5, BaBG-10, and 45S5-10 respectively (Two-way ANOVA followed by Bonferroni post-hoc test) 230
- Figure 6.8 Effect of BaBG on the (i) mRNA expression of TRPV1 and Cav2.2, and on (ii) the intracellular calcium level in the SN and SC. (ii). All values are in mean \pm SD (n=4 / group). ^ap<0.05, ^bp<0.05, ^cp<0.05, ^dp<0.05, ^ep<0.05, and ^fp<0.05 compared to control, CCI, BaBG-1, BaBG-5, BaBG-10, and 45S5-10 respectively. (One-way ANOVA followed by Tukey's multiple comparison post-hoc test) 233-234
- Figure 6.9 Effect of BaBG on S100b expression in the SN. Scale bar was set at 50 μ M with 20X magnification. All values are in mean \pm SD (n=3 rats/ group). ^ap<0.05, ^bp<0.05, ^cp<0.05, ^dp<0.05, ^ep<0.05, and ^fp<0.05 compared to control, CCI, BaBG-1, BaBG-5, BaBG-10, and 45S5-10 respectively. (One-way ANOVA followed by Tukey's multiple comparison post-hoc test) 236
- Figure 6.10 Effect of BaBG on S100b expression in the SC. Scale bar was set at 50 μ M with 20X magnification. All values are in mean \pm SD (n=3 rats/ group). ^ap<0.05, ^bp<0.05, ^cp<0.05, ^dp<0.05, ^ep<0.05, and ^fp<0.05 compared to control, CCI, BaBG-1, BaBG-5, BaBG-10, and 45S5-10 respectively. (One-way ANOVA followed by Tukey's multiple comparison post-hoc test) 236
- Figure 6.11 Effect of BaBG on GFAP expression in the SN. Scale bar was set at 50 μ M with 20X magnification. All values are in mean \pm SD (n=3 rats/ group). ^ap<0.05, ^bp<0.05, ^cp<0.05, ^dp<0.05, ^ep<0.05, and ^fp<0.05 compared to control, CCI, BaBG-1, BaBG-5, BaBG-10, and 45S5-10 respectively. (One-way ANOVA followed by Tukey's multiple comparison post-hoc test) 238

- Figure 6.12 Effect of BaBG on GFAP expression in the SC. Scale bar was set at 50 μ M with 20X magnification. All values are in mean \pm SD (n=3 rats/ group). ^ap<0.05, ^bp<0.05, ^cp<0.05, ^dp<0.05, ^ep<0.05, and ^fp<0.05 compared to control, CCI, BaBG-1, BaBG-5, BaBG-10, and 45S5-10 respectively. (One-way ANOVA followed by Tukey's multiple comparison post-hoc test) 239
- Figure 6.13 Effect of BaBG in the mRNA expression of GFAP, S100b, and NF-kB expression in the SN (i) and SC (ii). All values are in mean \pm SD (n=4 / group). ^ap<0.05, ^bp<0.05, ^cp<0.05, ^dp<0.05, ^ep<0.05, and ^fp<0.05 compared to control, CCI, BaBG-1, BaBG-5, BaBG-10, and 45S5-10 respectively. (One-way ANOVA followed by Tukey's multiple comparison post-hoc test) 242
- Figure 6.14 Effect of BaBG on TNF- α , IL-6, and IL-10 levels in the SN and SC. All values are in mean \pm SD (n=4 / group). ^ap<0.05, ^bp<0.05, ^cp<0.05, ^dp<0.05, ^ep<0.05, and ^fp<0.05 compared to control, CCI, BaBG-1, BaBG-5, BaBG-10, and 45S5-10 respectively. (One-way ANOVA followed by Tukey's multiple comparison post-hoc test) 243
- Figure 6.15 Molecular docking showing interaction of calcium (Ca²⁺) and barium (Ba²⁺) against S100b protein. 3D docking diagram of S100b bound to (i) Ca²⁺ and (ii) Ba²⁺ along with their (iii) binding potential 244
- Figure 6.16 Representative images of Golgi-Cox impregnated SC slice of control, CCI, BaBG-10, 45S5-10 and pregabalin treated rats. Scale bar was set at 200, 100, and 50 μ M with 4, 10, and 20X magnification 246
- Figure 6.17 (i) Representative image of the camera lucida drawing of neuron of SC which is superimposed over concentric circles using Sholl analysis. (ii) Effect of BaBG on (A), number of branching points (B) dendrite length across the soma, and (C) total length of dendrites. All values are in mean \pm SD (n=4 / group). ^ap<0.05, ^bp<0.05, and ^cp<0.05 compared to control, CCI, and BaBG-10 respectively. (One-way ANOVA followed by Tukey's post-hoc test) 247
- Figure 6.18 Effect of BaBG on NF-L expression in the SN. Scale bar was set at 50 μ M with 20X magnification. All values are in mean \pm SD (n=3 rats/ group). ^ap<0.05, ^bp<0.05, ^cp<0.05, ^dp<0.05, ^ep<0.05, and ^fp<0.05 compared to control, CCI, BaBG-1, BaBG-5, BaBG-10, and 45S5-10 respectively. (One-way ANOVA followed by Tukey's multiple comparison post-hoc test) 249
- Figure 6.19 Representative image of the histological analyses of SN stained with luxol fast blue at the end of 28th day post-surgery. The arrangement of nerve fibre is disrupted (shown in black) 249

	arrow) with high degree of myelin vacuolation (red star) in the disease group	
Figure 6.20	Effect of BaBG on (A) amplitude, (B) latency of CAP, and (C) MNCV. All values are in mean \pm SD (n=5 rats/ group). ^a p<0.05, ^b p<0.05, ^c p<0.05, ^d p<0.05, ^e p<0.05, and ^f p<0.05 compared to control, CCI, BaBG-1, BaBG-5, BaBG-10, and 45S5-10 respectively. (One-way ANOVA followed by Tukey's multiple comparison post-hoc test)	251
Figure 6.21	Representative images of the EMG recording in response to the cold-stimulus-evoked allodynia in control, CCI, BaBG-1, BaBG-5, BaBG-10, 45S5-10, and pregabalin treated rats	254
Figure 6.22	Representative images of the gastrocnemius muscle of the contralateral and ipsilateral side of the leg along with the histological analyses of gastrocnemius muscle stained with hematoxylin and eosin at the end of experimental protocol. Effect of BaBG on gastrocnemius muscle weight and cross-section area of muscle fiber. All values are in mean \pm SD (n=5 rats/ group). ^a p<0.05, ^b p<0.05, ^c p<0.05, ^d p<0.05, ^e p<0.05, and ^f p<0.05 compared to control, CCI, BaBG-1, BaBG-5, BaBG-10, and 45S5-10 respectively. (One-way ANOVA followed by Tukey's multiple comparison post-hoc test)	254
Figure 6.23	Showcases the specific objective's outcome in exploring the molecular mechanism behind the effect of BaBG in attenuating neuropathic pain (NP) in a CCI-induced NP rat model. It suggests that the development and progression of NP is associated with the enhanced calcium channel and TRPV1 expression that caused increase in the intracellular calcium and calcium-binding protein i.e., S100b level. These events led to glial cell activation that releases cytokine storm, thus exaggerating NP sensation. BaBG exhibited novel calcium regulating mechanism as it prolonged the repolarization phase of action potential. The Treatment with BaBG significantly reversed the NP phenotypes induced by CCI. Besides, CCI of peripheral nerve caused glial cell hyperactivation that was attenuated by BaBG. BaBG also lowered the S100B-induced increase in pro-inflammatory markers, specifically TNF- α and IL-6, in both the SC and SN post-injury	256
Figure 7.1	Summary and conclusion of the study	261

LIST OF TABLES

Table 1.1 Definition of the negative and positive symptoms observed clinically in patients suffering from neuropathic pain	14
Table 1.2 Clinical pharmacomanagement of neuropathic pain	25
Table 2.1 The chemical composition (mol %) of 45S5 and BaBG	45
Table 2.2 Brunauer–Emmett–Teller (BET) analysis results of 45S5 and BaBG	53
Table 2.3 Comparison of the important properties of 45S5 and BaBG	75
Table 3.1 Pharmacokinetic parameters for Ca released after single-dose oral administration of BaBG	94
Table 3.2 Pharmacokinetic parameters for Ba released after single-dose oral administration of BaBG	95
Table 3.3 Pharmacokinetic parameters for Si released after single-dose oral administration of BaBG	95
Table 3.4 Urinary and fecal excretion of Ca post-oral administration of BaBG in rats	98
Table 3.5 Urinary and fecal excretion of Ba post-oral administration of BaBG in rats	98
Table 3.6 Urinary and fecal excretion of Si post-oral administration of BaBG in rats	99
Table 3.7 Tissue concentration of Ca, Ba, and Si in the brain, heart, lungs, liver, kidneys, and spleen after single-dose oral administration of BaBG at doses 1, 5, and 10 mg/kg b.w. at days 1, 3, 5, and 7	104
Table 4.1 General observation and behavioral analysis during the first 4 h and 24 h after single-dose administration of BaBG and 45S5 (300 and 2000 mg/kg b.w.) in rats	118
Table 4.2 General observation and behavioral analysis after repeated-day administration of BaBG and 45S5 (50, 500, and 1000 mg/kg b.w.) in rats	130
Table 4.3 The organ coefficient of male and female rats after repeated 28 days oral administration of BaBG and 45S5 (50, 500, and 1000 mg/kg b.w.)	134

Table 4.4 The effect of repeated-dose 28 days oral administration of BaBG and 4S5 (50, 500, and 1000 mg/kg b.w.) on serum concentration of calcium, creatinine, CK-MB, ALP, ALT, and AST of male and female rats at the end of the experimental protocol.	136
Table 5.1 Primer sequences used for qRTPCR	164
Table 6.1 Primer sequences used for qRTPCR	217

LIST OF ABBREVIATIONS

ACC	: Anterior cingulate cortex
ACN	: Acetonitrile
ALP	: Alkaline phosphatase
ALT	: Alanine transaminase
AMY	: Amygdala
AST	: Aspartate transaminase
ASTM	: American society for testing and materials
AUC	: Area under curve
Ba(NO ₃) ₂	: Barium nitrate
BaBG	: Barium-doped bioactive glass
BBB	: Basso, Beattie, and Bresnahan
BCA	: Bicinchoninic acid
BET	: Brunauer–Emmett–Teller
BJH	: Barrett-Joyner-Halendra
Ca(NO ₃) ₂ .4H ₂ O	: Calcium nitrate tetrahydrate
CCBs	: Calcium channel blockers
CCI	: Chronic constriction injury
CCSEA	: Committee for the Control and Supervision of Experimentals on Animals
CL	: Clearance
C _{max}	: Maximum plasma concentration
CMC	: Carboxymethyl cellulose
CNS	: Central nervous system
CRE	: Creatinine
D	: Day
EDTA	: Ethylene diamine tetra acetic acid
EDX	: Energy dispersive Xray
ETS	: Experimental toe spreading
FBS	: Fetal bovine serum
FDA	: Food and Drug Administration
FTIR	: Fourier transform infrared spectroscopy
GFAP	: Glial fibrillary acidic protein
GIT	: Gastro intestinal tract
HA	: Hydroxyapatite
Hb	: Haemoglobin
HCA	: Hydroxy carbonated appetite
HCT	: Haematocrit
Iba-1	: Ionized calcium-binding adapter molecule 1
ICG	: International Commission on glass
ICP-MS	: Inductively coupled plasma mass spectrometry

IL 10	: Interleukin 10
IL-6	: Interleukin 6
IR	: Infrared
IUPAC	: International Union of pure and applied Chemistry
KBr	: Potassium Bromide
kV	: Kilo volt
LD ₅₀	: Lethal dose
LDH	: Lactate dehydrogenase
LPS	: Lipopolysaccharide
LTP	: Long term potentiation
mA	: Milli ampere
MBP	: Myelin basic protein
MCHC	: Mean cell haemoglobin concentration
MCV	: Mean corpuscle volume
MHC	: Major histocompatibility complex
MRT	: Mean Residence Time
NaNO ₃	: Sodium nitrate
NBO	: Non bridging oxygen
NF	: Neurofilament
NF- κ B	: Nuclear factor kappa B
NOAEL	: No observed adverse effect level
NP	: Neuropathic pain
NPL	: Normal foot print length
NTS	: Normal toe spreading
OECD	: Organization for Economic Cooperation and Development
OFT	: Open field test
PBS	: Phosphate buffer saline
PL	: Print length
PNS	: Peripheral nervous system
PPM	: Parts per million
qRT-PCR	: Quantitative Real-Time polymerase chain reaction
RAGE	: Receptor for advanced glycated end product
RBC	: Red blood corpuscle
RDW	: Red blood cell distribution
RVM	: Rostroventral medulla
SAED	: Selected area electron diffraction
SBF	: Simulated body fluid
SC	: Spinal cord
SD	: Standard deviation
SEM	: Scanning electron microscopy
SFI	: Sciatic functional index
SN	: Sciatic nerve

$t_{1/2}$:	Half life
TBI	:	Traumatic brain injury
TCO4	:	Technical committee 4
TEM	:	Transmission electron microscopy
TEOS	:	Tetraethyl orthosilicate
TEP	:	Triethyl phosphate
TH	:	Thalamus
TLR 4	:	Toll like receptor 4
T_{max}	:	Total time required to reach maximum plasma concentration
TMZ	:	Temozolomide
TNF- α	:	Tumour necrosis factor-alpha
TRIS	:	Trihydroxy methyl aminomethane
TRPV1	:	Transient receptor potential Vanilloid-1
TS	:	Total spreading
TT	:	Distance between intermediary toes
VEGF	:	Vascular endothelial growth factor
VGCC	:	voltage-gated calcium channel
V_z	:	Volume of distribution
WBC	:	White blood cells
XRD	:	X-ray diffractometry

PREFACE

The thesis's research work entitled "**Novel calcium-regulating mechanism of barium-doped material for the treatment of neuropathic pain**" is based on the assessment of the calcium-regulating mechanism of barium-doped biomaterial and its pharmacological potential for the treatment of neuropathic pain (NP) using chronic constriction injury (CCI) model. NP is a prominent clinical illness that arises as a consequence of injury to the somatosensory nervous system leading to either spontaneous or evoked pain. Globally, NP affects 7-10 % of people worldwide. Despite over a century of studies on nociception, the current treatments for chronic pain have limited effectiveness with adverse effects, leading to withdrawal and poor quality of life. Currently, calcium channel blockers (CCBs) are the first-line treatment for NP. The clinically prescribed CCBs include pregabalin and gabapentin which are organic in nature. Unlike inorganic compounds, organic compounds have various protein interactions which are linked to significant adverse effects. Therefore, it is imperative to develop novel therapeutic strategies that would work on calcium channels. We have selected an inorganic compound i.e., barium-doped bioactive glass (BaBG) that may have certain advantages over the organic compounds as barium that is doped in BaBG are endogenously present in the body so they may not pose any undesired effects. Besides, barium is present in exoplanets so we have evolved containing barium within us. Thus, BaBG was synthesized using the wet chemistry method i.e., sol-gel method. By using the *ex vivo* electrophysiological technique, the calcium-regulating properties of BaBG via its action on the calcium channel were assessed. Further, to examine its potential regenerative and anti-inflammatory properties, cell line-based studies were performed. To assess the therapeutic potential of BaBG for the treatment of NP, a

comprehensive calcium-modulating molecular mechanism was performed in CCI-induced NP in rats. In extension, the sensory and motor abnormalities developed post-CCI was evaluated using a variety of pain behavioral assessment tests. The synaptic rewiring occurring post-BaBG treatment was also examined by tracing the neurons. Furthermore, the *in vivo* biodistribution of the dopants leached from BaBG was determined using quantitative analytical techniques such as inductively coupled plasma mass spectrometry (ICP-MS) as BaBG not only contains barium under the permissible physiological limits but also has other elements that are involved in various physiological activities. By employing a multidisciplinary approach encompassing materials science, pharmacology, and toxicology, we strived to harness the unique properties of BaBG for the development of therapeutic interventions for NP. The entire work has been compiled into seven chapters: **Chapter 1** describes the introduction and significance of the present study. **Chapter 2** describes the synthesis and characterization of barium-doped bioactive glass (BaBG), investigating its *in vitro* regenerative and anti-inflammatory potential. **Chapter 3** describes the *in vivo* pharmacokinetics, biodistribution, and excretion of dopants released from BaBG following oral administration. **Chapter 4** describes the oral acute and sub-acute toxicity study of BaBG according to the OECD guidelines. **Chapter 5** describes the temporal changes in the intracellular calcium and S100b protein levels in the pathophysiology of CCI-induced NP in rats. **Chapter 6** describes the pharmacological evaluation of BaBG in the treatment of NP. **Chapter 7** summarizes the entire study completed with its essential outcomes.